DOI: 10.1002/ ((please add manuscript number))
Article type: Communication

Promoting the Transformation of Li_2S_2 to Li_2S: Significantly Increasing Utilization of Active Materials for High Sulfur Loading Li-S Batteries

Xiaofei Yang+, Xuejie Gao+, Qian Sun, Sara Panahian Jand, Ying Yu, Yang Zhao, Xia Li, Keegan Adair, Liang-Yin Kuo, Jochen Rohrer, Jianneng Liang, Xiaoting Lin, Mohammad Norouzi Banis, Yongfeng Hu, Hongzhang Zhang, Xianfeng Li, Ruying Li, Huamin Zhang*, Payam Kaghazchi, Tsun-Kong Sham, Xueliang Sun**

Dr. X. Yang, X. Gao, Dr. Q. Sun, Dr. Y. Zhao, Dr. X. Li, K. Adair, J. Liang, X. Lin, Dr. M. Bains, R. Li, Pro. X. Sun
Department of Mechanical and Materials Engineering
University of Western Ontario, London, Ontario, N6A 5B9, Canada
E-mail: xsun@eng.uwo.ca (X. Sun)

X. Yang, Y. Yu, Prof. H. Zhang, Prof. X. Li, Prof. H. Zhang
Division of Energy Storage
Dalian Institute of Chemical Physics
Chinese Academy of Sciences
Zhongshan Road 457, Dalian 116023, China
E-mail: zhanghz@dicp.ac.cn, zhanghm@dicp.ac.cn

S. P. Jand, L.-Y. Kuo, Prof. P. Kaghazchi,
Theoretical Electrochemistry, Physikalische und Theoretische Chemie
Freie Universität, Berlin, Takustr. 3, D-14195 Berlin, Germany

Dr. Y. Hu
Canadian Light Source
44 Innovation Boulevard, Saskatoon, SK, S7N 2V3, Canada

X. Gao, Prof. T.-K. Sham,
Department of Chemistry
University of Western Ontario, ON, N6A 5B9, Canada

J. Rohrer
Institut für Materialwissenschaft, Fachgebiet Materialmodellierung,
Technische Universität Darmstadt, Otto-Berndt-Str. 3, 64287 Darmstadt, Germany

X. Yang Y. Yu,
University of Chinese Academy of Sciences
Beijing 100049, China

Prof. P. Kaghazchi
Forschungszentrum Jülich GmbH
Institute of Energy and Climate Research, IEK-1, D-52425 Jülich, Germany

+ X. Yang and X. Gao contributed equally to this work

Keywords: Amorphous cobalt sulfide; High loading; Catalytic effect; High utilization; Lithium-sulfur batteries;

Lithium-sulfur (Li-S) batteries with high sulfur loading are urgently required in order to take advantages of their high theoretical energy density. Ether-based Li-S batteries involve the sophisticated multi-step solid-liquid-solid-solid electrochemical reaction mechanisms. Recently studies on Li-S batteries have widely focused on the initial solid (sulfur)-liquid (soluble polysulfide)-solid (Li_2S_2) conversion reactions, which contributes to the first 50% of the theoretical capacity of the Li-S batteries. Nonetheless, the sluggish kinetics of the solid-solid conversion from solid-state intermediate product Li_2S_2 to the final discharge product Li_2S (corresponding to the last 50% of the theoretical capacity) leads to the premature end of discharge, resulting in low discharge capacity output and low sulfur utilization. To tackle the aforementioned issue, a catalyst of amorphous cobalt sulfide (CoS_3) was proposed to decrease the dissociation energy of Li_2S_2 and propel the electrochemical transformation of Li_2S_2 to Li_2S. The CoS_3 catalyst plays a critical role in improving the sulfur utilization, especially in high-loading sulfur cathodes (3~10 mg cm^{-2}). Accordingly, the Li_2S/Li_2S_2 ratio in the discharge products increased to 5.60/1 from 1/1.63 with CoS_3 catalyst, resulting in a sulfur utilization of 20% (335 mAh g^{-1}) increase compared to the counterpart sulfur electrode without CoS_3.

Lithium-sulfur batteries with a high theoretical energy density of 2600 Wh kg^{-1} have received great attention and have been considered as one of the most promising energy storage devices. [1, 2, 3] During the past ten years, most efforts have been focused on solving the “shuttle effect” resulting from the dissolution of polysulfides, the volumetric expansion during lithiation and low conductivity of S/Li_2S. [4] However, the sulfur utilization, another important parameter for high-energy-density was overlooked due to the well-designed materials/structures with relatively low sulfur loadings (<2 mg cm^{-2}) and excellent capability in Li^+/e^- transportation. [5]

In the typical Li-S batteries using prevailing ether electrolytes, the active sulfur cathode undergoes multi-step electrochemical reactions through solid-liquid-solid-solid phase transformation during the discharge process [1, 6]. Based on the most widely accepted state-of-the-art understanding on the reaction mechanism of ether-based Li-S batteries, a tri-stage reaction process takes place in the discharge process as shown in Figure S1. At the high potential regime above 2.1 V, S_8 is reduced through a stepwise sequence of lithium polysulfides to Li_2S_4, which delivers 25% of the theoretical capacity (418 mAh g^{-1}) corresponding to a 1/2 electron transfer process per S atom (i.e. 4e^- per S_8). This is a solution-mediated reaction dominant and fast-dynamic step owing to a series of soluble polysulfides involved. At the second stage, a relatively low dynamic liquid-solid reaction, corresponding to the further reduction of Li_2S_4 to Li_2S_2, contributing to another 25% of the theoretical capacity, occurs due to the high energy barrier for solid-state Li_2S_2 nucleation to be overcome. Finally, the solid-solid conversion of Li_2S_2 to Li_2S, the most difficult and the rate-controlling step, proceeds at the third stage, which has the potential to deliver the last 50% theoretical capacity, in theory, equaling to a capacity of 836 mAh g^{-1}. [7] However, the interconversion is significantly hindered by the sluggishness of solid-state diffusion, thus leading to the premature end of discharge and low sulfur utilization, which results in a huge deviation between the practical capacity delivered and the theoretical value. [8] The situation is even worse for high sulfur loading cathodes, which is the essential component for high-energy-density Li-S batteries, due to poor Li^+/e^- transportation. [9, 10] According to the statistical information from current research on Li-S batteries with more than 4 mg cm^{-2} of high sulfur loadings, only 13.6% of the batteries can deliver high initial capacities of more than 1200 mAh g^{-1}, corresponding to 71.7% sulfur utilization. Due to both low sulfur utilization and serious capacity decay during cycling, only 5.3% of them maintain capacities over 1000 mAh g^{-1} within no more than 100 cycles.[2] In this consideration, increasing the sulfur utilization is of significance for paving the way for high-energy-density Li-S batteries.

Amorphous metal sulfides (MS_x) exhibit non-periodic regular arrangement of atoms with large amounts of dangling bonds on the surface (which can be utilized as active sites), enabling them with different electrochemical performance and catalytic effect compared with the crystalline sulfides. [11] Recently, the MS_x such as TiS_4 and MoS_3 with sulfur-like behavior was successfully applied as the active materials for Li-S batteries. [12] Due to the large reversible specific capacity and the inability to form soluble polysulfides during the charge/discharge process, the Li-S batteries assembled with MS_x exhibited excellent cycling performance in carbonate electrolytes. However, the catalytic effect of MS_x in Li-S batteries remains elusive, to the best of our knowledge, despite the effectiveness of catalytic MS_x (eg. CoS_x, MoS_x) species that have been repeatedly demonstrated in other electrochemical fields such as SEI formation in Na-ion batteries, hydrogen evolution reaction (HER) and oxygen evolution reaction (ORR). [13]

Herein, we propose the use of amorphous CoS_3 as a catalyst to improve the reaction kinetics for the transformation from Li_2S_2 to Li_2S. The catalytic effect is unequivocally demonstrated by both electrochemical performance and X-ray absorption spectroscopy results and the detailed catalytic mechanism is further clarified by density functional theory (DFT) calculations. Beneficial from High sulfur utilization of more than 80% for high sulfur loading cathodes of 3~10 mg cm^{-2} is realized with CoS_3 which is 20% more than that for the cathodes without CoS_3. Additionally, the catalytic effect is well maintained during long-term charge/discharge processes. Capacities of 1008, 1047 and 1076 mAh g^{-1} are maintained for 3, 6 and 10 mg cm^{-2} sulfur loaded electrodes after 100, 70 and 50 cycles at a current density of 1.3 mA cm^{-2}, respectively, which are 60%, 77%, 111% higher than their counterparts. This work will open a new window in catalysis to improve the electrochemical performance of high sulfur loading Li-S batteries.

Firstly, the nitrogen-doped carbon nanotubes (NCNTs) growing on carbon paper (CP), labeled as CP@NCNT, is chosen as support for loading the catalyst. The detailed synthesis process can be seen from Figure 1a. Firstly, the cobalt-based metal organic frames (Co-MOF), acting as the precursor, were grown on the surface of CP@NCNT. Afterward, the Co-MOF was further transformed into the CoS_3 (the ratio of cobalt to sulfur is determined by the energy dispersive X-ray spectrometry (EDS) and atomic ratio shown in Figure S2 and Table S1) with the assistance of thioacetamide (TAA). Before MOF growth and CoS_3 loading, the NCNTs show an aligned bamboo structure with smooth surface and diameters of approximately 20~50 nm according to the SEM and TEM images are shown in Figure S3. After Co-MOF growth (Figure S4) and the sulfidation processes, an ultrathin amorphous CoS_3 film with thicknesses around 5~10 nm (except a few agglomerated particles shown in Figure S5), according to the X-ray diffraction (XRD) results and scanning electron microscopy (SEM) and transmission electron microscopy (TEM) images shown in Figure S6 and Figure 1b-k, is anchored on the surface of NCNTs (labelled as CP@NCNT@CoS_3). After sulfur impregnation, as shown in Figure S7 and Figure S8, there are no large sulfur particles on the surface of S/CP@NCNT and S/CP@NCNT@CoS_3 composites. Furthermore, the sulfur, carbon, and cobalt show the same distribution in elemental mappings, indicating that the sulfur is uniformly dispersed in the scaffolds of the CP@NCNT and CP@NCNT@CoS_3.[14] The uniformly dispersed sulfur has access to an extensive electron transport network as fabricated by the NCNTs arrays. Moreover, the CoS_3 acts as an effective polysulfide immobilizer via chemical adsorption as well as applies as a catalyst for the conversion of Li_2S_2 to Li_2S, improved cycling performance and sulfur utilization should be expected.

The influence of CoS_3 on the electrochemical reactions is investigated by the cyclic voltammograms (CV) profiles and electrochemical impedance spectroscopy (EIS) curves. As shown in Figure 2a, both S/CP@NCNT and S/CP@NCNT@CoS_3 electrodes show typical CV profiles with two cathodic peaks and one anodic peak, corresponding to the two-step reduction of sulfur to Li_2S_2/Li_2S and reversible oxidation of Li_2S/Li_2S to sulfur.[15, 16] It is noteworthy that the potential difference between the anodic peak and cathodic peak at around 2.0 V of

$S/CP@NCNT@CoS_3$ electrode is 0.45 V, which is much smaller compared with S/CP@NCNT electrode (0.52 V), suggesting fast electrochemical reaction kinetics for $S/CP@NCNT@CoS_3$ electrode. This phenomenon can be further explained by the EIS curves. As shown in Figure 2b, the $S/CP@NCNT@CoS_3$ electrode (10.89 Ω cm^{-2}) exhibits large ohmic resistance (R_s) compared with S/CP@NCNT electrode (5.19 Ω cm^{-2}), which is mainly resulted from the low electronic conductive CoS_3 that decreased the electronic conductivity of the whole electrode. However, it should be noted that the charge transfer resistance (R_{ct}), a parameter closely related to the chemical reaction activation energy, of $S/CP@NCNT@CoS_3$ electrode (35.09 Ω cm^{-2}) is only 30% of its counterpart (117.14 Ω cm^{-2}), suggesting faster electrochemical kinetics with CoS_3 loading. It can be assumed that the CoS_3 can catalyze the electrochemical reactions, either for the whole charge/discharge process or at least for some steps. The catalytic effect is further demonstrated by the CV results of Li_2S_6-Li_2S_6 symmetrical cells shown in Figure 2c. It can be clearly seen that the current density significantly increases by 2.5 times with CoS_3, suggesting that CoS_3 can accelerate the electrochemical reactions of lithium polysulfides. [17, 18]

The catalytic effect of CoS_3 is further investigated by the charge/discharge behavior at a current density of 1.3 mA cm^{-2}. As shown in Figure 2e~f, the $S/CP@NCNT@CoS_3$ electrode shows three plateaus in the voltage window of 1.7~2.8 V. The two typical plateaus at around 2.3 V and 2.1 V can be attributed to the two-step reduction from sulfur to Li_2S, while the additional plateau at around 1.88V belongs to the CoS_3 reduction reaction. (Figure S9). As it can be seen, the $S/CP@NCNT@CoS_3$ electrode delivers a capacity of 417 mAh g^{-1} at the first plateau around 2.3 V, which is a 37 mAh g^{-1} increase compared with the S/CP@NCNT electrode. This phenomenon likely arises from the improved interaction between the CoS_3 and polysulfides, leading to the limitation of polysulfide diffusion and improved polysulfide reduction. To confirm the strong CoS_3-polysulfide interaction, Li_2S_4 is chosen as the adsorbate for static adsorption. As shown in Figure S10, $NCNT@CoS_3$ in the polysulfide solution leads to a clear and transparent solution color, while NCNTs show no observable effect and the solution color remains the yellow color of Li_2S_4. The significant difference further demonstrates the enhanced affinity of polysulfides to CoS_3. [17, 19] Following the first discharge plateau, an obvious valley appears between the first plateau and the second plateau, which is called the Li_2S nucleation point. [20] The potential difference between the Li_2S nucleation point and the tangential line of the potential plateau is used to evaluate the Li_2S nucleation kinetics. The S/CP@NCNT electrode shows a large overpotential of 35 mV, which suggests that a high interfacial energy barrier existed for Li_2S nucleation and deposition on the surface of CP@NCNT electrode. In contrast, the Li_2S nucleation behavior is quite different with CoS_3 loading. The S/CP@NCNT@CoS_3 electrode exhibits a significantly reduced interfacial energy barrier of 9 mV, ~25% of that of the S/CP@NCNT electrode, indicating the facilitation of Li_2S nucleation and deposition process with CoS_3 assistance. [20] More eye-catching results can be seen from the second plateau, corresponding to Li_2S_4 to Li_2S transition. For the S/CP@NCNT electrode, the polarization increases rapidly at the end of the discharge and results in terminated discharge after a few seconds, which mainly results from the solid-solid transformation from Li_2S_2 to Li_2S. On the contrary, the second plateau is obviously prolonged and the polarization is gradually increased at the end of discharge for S/CP@NCNT@CoS_3 electrode, which suggests that the transfer process from Li_2S_2 to Li_2S is moderate and easier to realize with CoS_3 assistance. In this consideration, more Li_2S_2 produced during discharge can be transformed into the final discharge product (Li_2S) and high sulfur utilization is obtained. Besides the capacity contributed by the $LiNO_3$ decomposition (~1.7 V) and CoS_3 reduction (~1.88 V) for S/CP@NCNT and S/CP@NCNT@CoS_3 electrodes, respectively, an increase of capacity of 313 mAh g^{-1} (933 mAh g^{-1} vs 620 mAh g^{-1}) is delivered by the S/CP@NCNT@CoS_3 electrode compared with the S/CP@NCNT electrode at the second plateau, which is of significance for high energy density Li-S batteries. The increased sulfur utilization and Li_2S formation with CoS_3 is further demonstrated by the onset potential of discharge curves and Li_2S activation peaks. As shown in Figure 2e, the shows an onset potential of 1.99 V (below the second plateau), while the onset potential for the S/CP@NCNT electrode is 2.22 V (in the first plateau). The onset potential difference indicates that more reductive materials versus Li are produced on the cathode side. Moreover, higher Li_2S active energy and longer active time are exhibited for S/CP@NCNT@CoS_3 electrode (Figure 2e), indicating more Li_2S produced during the discharge process. Additionally, it is noteworthy that the catalytic effect of CoS_3 remains intact during repeated charge/discharge processes. As shown in Figure S11, after 20 cycles, the S/CP@NCNT@CoS_3 electrode still shows lower onset potential, higher Li_2S active energy, longer active time and higher discharge capacity compared with the S/CP@NCNT electrode (1228 mAh g^{-1} vs. 668 mAh g^{-1}), which is of significance in maintaining the Li-S batteries with high energy density during long-term cycling. In this regard, as shown in Figure 2d, the Li-S batteries assembled with S/CP@NCNT@CoS_3 can retain a high discharge capacity of 1008 mAh g^{-1} after 100 cycles, which is 60% more than that of the S/CP@NCNT electrode (630 mAh g^{-1} after 100 cycles). To meet the requirements for practical application, the long-term cycling performance of Li-S batteries assembled with S/CP@NCNT@CoS_3 electrode is also investigated at a current density of 4 mA cm^{-2}. As shown in Figure 2g, after fast capacity decay in the first two cycles, a high capacity of around 1300 mAh g^{-1} is achieved at the 3rd cycle and a high capacity of around 680 mAh g^{-1} is maintained after 400 cycles, further demonstrating the high sulfur utilization and cycling performance with CoS_3 catalyst.

Considering the high sulfur utilization and high capacity retention of the S/CP@NCNT@CoS_3 electrode, the electrochemical performance of Li-S batteries assembled with higher sulfur loaded S/CP@NCNT@CoS_3 electrodes are investigated. Moreover, inorder to achieve high practical energy density, low electrolyte/sulfur (E/S) ratios are controlled as 9.6 μL mg^{-1} and 5.7 μL mg^{-1} for the 6 mg cm^{-2} and 10 mg cm^{-2} sulfur loaded-electrode testing. [21] As shown in Figure 2h-i, the Li-S batteries assembled with higher sulfur loadings of 6 mg cm^{-2} and 10 mg cm^{-2} deliver high capacities of 1601 mAh g^{-1} at the first cycle and 1172 mAh g^{-1} at the nineteenth cycle, and can maintain high capacities of 1047 mAh g^{-1} and 1076 mAh g^{-1} after

70 and 50 cycles, respectively. These specific capacities are 77% and 111% increases compared with their respective counterparts (593 mAh g^{-1} for 6 mg cm^{-2} S/CP@NCNT electrode and 510 mAh g^{-1} for 10 mg cm^{-2} S/CP@NCNT electrode). The high initial capacities and excellent retention after cycling for the 6 mg cm^{-2} and 10 mg cm^{-2} sulfur loaded S/CP@NCNT@CoS_3 are huge improvements compared to the literature results with similar sulfur loadings and cycling life, as listed in Table S2 and Figure S12. [9, 16, 22] The charge/discharge curves of the Li-S batteries assembled with 6 mg cm^{-2} and 10 mg cm^{-2} (Figure S13) exhibit the similar catalytic characteristics (long second plateau, low one-set potential, high Li_2S active energy, low overpotential and long active time), further highlight the effective catalytic effect of CoS_3 for high sulfur loading electrodes. As shown in Figure S13, the S/CP@NCNT@CoS_3 and S/CP@NCNT electrodes show similar ovepotentials of 0.08 V (sulfur loading:6 mg cm^{-2}) and 0.15 V (10 mg cm^{-2}) at the first discharge plateau, corresponding to the sulfur to Li_2S_4. However, the overpotentials are obviously decreased with CoS_3 catalyst at the second discharge plateau, which are 0.17 V and 0.25 V for 6 mg cm^{-2} and 10 mg cm^{-2} sulfur loaded S/CP@NCNT@CoS_3 electrodes, respectively, which are 0.03 V and 0.10 V smaller than their counterparts without CoS_3 catalyst. Compared with Coulombic efficiency (CE) that have been widely applied in Li-S batteries systems, the Energy efficiency (EE) maybe more appreciate in evaluating the electrochemical reversibility of Li-S batteries. [23] Because it takes the overpotential into consideration. The EEs of the Li-S batteries assembled with S/CP@NCNT@CoS_3 and S/CP@NCNT electrodes are shown in Figure S14. Due to lower overpotentials at the second discharge plateau, higher EEs of around 90% and 86% are achieved by 6 mg cm^{-2} and 10 mg cm^{-2} sulfur loaded S/CP@NCNT@CoS_3 electrodes, which are 2% and 5% higher than their counterpart without CoS_3 catalyst. The higher energy utilization of S/CP@NCNT@CoS_3 electrode further highlights the important role of the CoS_3 played in Li-S batteries.

To investigate the effect of CoS_3 on improving the sulfur utilization, the morphology and composition of discharge products on CP@NCNT@CoS_3 and CP@NCNT electrodes after washed with a solvent of 1, 2-dimethoxymethane (DME) are investigated by SEM and X-ray photoelectron spectroscopy (XPS). As shown in Figure 3a-d, a thin layer of discharge products is deposited on the surface of the CP@NCNT electrode. The discharge products are further investigated by XPS and the S 2p spectra are exhibited in Figure 3e. The S 2p spectra is a doublet comprised of closely spaced spin-orbit components owing to 2p3/2 and 2p1/2. Each sulfur compound presents the characteristic doublet, and only the high-intensity 2p3/2 will be discussed in the following section for simplicity. The peaks located at 169.0 and 167.2 are assigned to R-SO_2-R/SO_4^{2-} and $S_2O_3^{2-}$/SO_3^{2-}, respectively, which mainly results from the oxidization of sulfur species during sample transfer or the residual bis(trifluoromethylsulfonyl) imide (LiTFSI). Deconvolution of S 2p spectra under the broad sulfide region provides three unique components, belonging to bridging sulfur (S_B^0) in the polysulfide sulfides or sulfur at 163.5 eV terminal sulfur (S_T^{1-}) at 162.0 eV and sulfide dianion (S^{2-}) in Li_2S at 160.4 eV, respectively (Figure S15). [24] For S/CP@NCNT electrode, all three components are exhibited in the S 2p spectra (Figure 3e). Considering the electrode for XPS was washed with DME and most of the soluble polysulfides are removed. We can deduce that the S_T^{1-} and S_B^0 mainly belong to Li_2S_2 and unutilized sulfur. Due to the incomplete electrochemical reaction, the S/CP@NCNT delivers a low discharge capacity. On the contrary, as shown in Figure 3f-i, more insoluble products are observed on the surface of the S/CP@NCNT@CoS_3 electrode and the products show an island morphology. In the S 2p spectra (Figure 3j), only two components are observed, where S_T^{1-} belongs to Li_2S_2 and S^{2-} assigns to Li_2S. It should be noted that the peak area ratio of S^{2-} to S_T^{1-} in S/CP@NCNT electrode is 1/1.63, which raises to 5.60/1, indicating more Li_2S produced with CoS_3 assistance. In other words, CoS_3 is helpful for conversing Li_2S_2 to Li_2S and improving the sulfur utilization and discharge capacity output. To explore the reasons for the improved cycling stability of S/CP@NCNT@CoS_3 electrode, the morphology of S/CP@NCNT@CoS_3 and S/CP@NCNT electrodes after 100 cycles are investigated. As shown in Figure S16 a~c, similar to the morphology of the 1st cycle, insoluble products with an island morphology are maintained on the surface of the S/CP@NCNT@CoS_3 electrode, suggesting that the CoS_3 maintains its electrochemical activity during repeated charge/discharge processes. On the contrary, a passivating layer is deposited on the surface of the S/CP@NCNT electrode (Figure S17 a~c) and almost all of the Li^+ transport channels are blocked, which is mainly attributed to the low chemical interaction between polysulfides and NCNT and results in the poor cycling stability. [19] The difference is further demonstrated by the thickness of passivating layer on the Li anode surface. As shown in Figure S16 d~f, the thickness of passivating layer on Li anode coupled with S/CP@NCNT@CoS_3 electrode is 17 μm, which is only 27% of Li anode coupled with S/CP@NCNT electrode (64 μm, Figure S17 d~f) further demonstrated the catalytic effect and strong chemical interaction of CoS_3 catalyst.

To further understand the catalytic mechanism of CoS_3, in-situ synchrotron-based X-ray absorption near edge structure (XANES) measurements are conducted in an ether-based electrolyte with $LiClO_4$ as lithium salt within a custom-designed in-situ testing cell (Figure S18). The results from the sulfur K-edge and cobalt K-edge XANES are displayed in Figure 4. Before charge/discharge processes, a feature at 2472.0 eV is presented for both sulfur K-edge XANES of S/CP@NCNT@CoS_3 and S/CP@NCNT electrodes, which is attributed to the S 1s to S-S π^* state transition of elemental sulfur.[25, 26] With the depth of discharge, a weak pre-edge feature at 2470.1 eV emerges, which can be assigned to the S 1s to π^* state transition associated with linear polysulfides.[25, 27, 28]. Moreover, the pre-edge at 2470.1 gradually picks up the intensity at the expense of the feature at 2472.0 eV which becomes weaker, suggesting decreasing chain length with the depth of discharge. At the inflection point of second discharge plateau (the light pink point in the discharge profile), the intensity of the pre-edge is the highest, indicating the formation of Li_2S_2 with the lowest chain length. [28] After that, two features at 2473.0 eV and 2475.3 eV, assigned to Li_2S [27, 29] appear with decreasing intensity of the pre-edge feature at 2470.1 eV, indicating the transformation from Li_2S_2 to Li_2S. However, for the S/CP@NCNT electrode, due to the polarization increase at the inflection point, the discharge process terminates within a few seconds, resulting in the incomplete transformation from Li_2S_2 to Li_2S (as illustrated in Figure 4d). As shown in Figure S19 and Figure 4b, at the end of discharge, both polysulfides feature at 2470.1 eV and Li_2S features at 2473.0 eV and 2475.6 eV are observed in the sulfur K-edge XANES of S/CP@NCNT, indicating that only a fraction of polysulfides is converted into Li_2S, which is coincided well with the low sulfur utilization of S/CP@NCNT electrode. In contrast, for the S/CP@NCNT@CoS_3 electrode, the feature associated with polysulfides disappears and only two Li_2S features remain at the end of discharge, further demonstrating the contribution of CoS_3 in increasing the sulfur utilization (as illustrated in Figure 4c). Beneficial from the complete transformation from polysulfides to the final discharge product of Li_2S, high sulfur utilization and high capacity output are achieved, which is coincided well with the electrochemical performance shown in Figure 2. The high sulfur utilization with the assistance of CoS_3 is further demonstrated by observing the difference of separators after the first discharge. As shown in Figure S20, the separator of S/CP@NCNT electrode exhibits the typical color of polysulfides, indicating the existence of polysulfides at the end of discharge. On the contrary, the separator of S/CP@NCNT@CoS_3 remains its original color, demonstrating that all polysulfides were successfully converted into the insoluble Li_2S. These results coincide well with the XANES results. Additionally, a sulfur feature at 2472.0 eV can be observed in the sulfur K-edge XANES of S/CP@NCNT@CoS_3 at the end of the charge process, demonstrating that Li_2S can be fully oxidized into the sulfur at the following charge process, which is meaningful for the following cycling. The role of CoS_3 in increasing sulfur utilization is explored by the Co K-edge XANES. As shown in Figure 4a and Figure S21, before the discharge/charge process, a peak is presented at 7725.8 eV and a pre-edge feature is observed at 7711.1 eV, which can be assigned to Co^{2+}, and is in good agreement with the reference samples shown in Figure S22. During the discharge process, the feature gradually shifts to higher energy, which is mainly a result of the strong interactions between the Co^{2+} and sulfur species. During the charge process, a reversible process is observed, and the feature gradually shifts back to 7725.8 eV. In other words, the CoS_3 can anchor the sulfur species on its surface and enable the reversible transformation between sulfur and Li_2S.

To understand the catalytic mechanism of CoS_3 at the atomic level, first-principle calculations based on DFT were further performed. In these calculations, we study the adsorption of the model polysulfide Li_2S_2 on CoS_3 and NCNT surfaces. For details on the preparation of the amorphous CoS_3 surface slabs, we refer to the Supporting Information document, in particular to Figure S23. To find the most favorable structure of Li_2S_2/CoS_3, we first calculate total energies for a Li_2S_2 monomer adsorbed at six distinguishable sites at each side of three different surface slabs (6×3×2=36 structures in total). Figure 5a details the most favorable optimized atomic structure of adsorbed Li_2S_2 on the CoS_3 surface. It is found that the Li_2S_2 molecule remains almost intact on the CoS_3 surface after geometry relaxation. As shown in Figure 5a-b, the adsorption energy (E_a) of Li_2S_2 on CoS_3 is -3.47 eV, which is much stronger than the E_a of Li_2S_2 on the NCNT (-2.39 eV). This result suggests a strong interaction between polysulfides and CoS_3, which is in good agreement with the static adsorption results in Figure S10. More specifically, the dissociation energy (ΔE) of Li_2S_2 is, for the first time, calculated to estimate the energy barrier for the conversion from Li_2S_2 to Li_2S. To find the minimum energy structure of detached Li_2S_2, we have considered 10 configurations with detached S binding at neighbored sites. The following discussion is based on the minimum-energy structure. As shown in Figure 5a-b, the S-S bond length in Li_2S_2 is 2.01 Å. After increasing the distance of the S-S bond to 2.85 Å or 3.08 Å, the S-S bond is dissociated, and the energy difference is called the dissociation energy. As can be seen, the ΔE of Li_2S_2 on CoS_3 is 0.93 eV, while the relative value on NCNT is 2.74 eV. In other words, it is easier for Li_2S_2 on the CoS_3 to break the S-S bond to form Li_2S, suggesting the powerful effect of CoS_3 in catalyzing the interconversion of Li_2S_2 to Li_2S. It is helpful for understanding why the polarization is gradually increased at the end of discharge for S/CP@NCNT@CoS_3 electrodes, while the polarization increases rapidly at the end of the discharge and results in terminated discharge after a few seconds for S/CP@NCNT electrodes (Figure S11 and Figure S13). The detailed conversion process from sulfur to final discharge product of Li_2S is illustrated in Figure 5c. Firstly, the S_8 is partially reduced by the e^- and Li^+ and is transformed into long-order polysulfides such as Li_2S_6 and Li_2S_4. Such polysulfides show strong chemical interaction with CoS_3 and can be anchored on the surface of CoS_3. The long-chain polysulfides are further reduced to solid Li_2S_2. Interestingly, due to the lower dissociation energy of Li_2S_2 on the surface of CoS_3, Li_2S_2 can be easily converted into Li_2S, resulting in high sulfur utilization, fast capacity output, and good cycling performance.

In summary, we have proposed and developed a novel approach to use amorphous CoS_3 as an effective catalyst for the solid-solid electrochemical conversion of Li_2S_2 to Li_2S, which significantly improves the sulfur utilization of high sulfur loading electrodes. The CoS_3 shows strong interaction with the sulfur species, thus enabling the anchoring of the sulfur species on its surface and ensures the reversible transformation among sulfur species. Additionally, the Li_2S_2 shows lower dissociation energy on the surface of CoS_3, facilitating the conversion of Li_2S_2 to Li_2S. The high sulfur loaded electrodes (3~10 mg cm^{-2}) with CoS_3 exhibit more than 80% sulfur utilization, which is more than a 20% increase compared to their counterparts without CoS_3. Additionally, the catalytic activity of the CoS_3 catalyst remains effective during repeated cycling, and thus ensures the high capacity retention for long cycle life. The S/CP@NCNT@CoS_3 electrodes with 3, 6 and 10 mg cm^{-2} sulfur deliver high capacities of 1008 mAh g^{-1}, 1047 mAh g^{-1}, and 1075 mAh g^{-1} after 100, 70 and 50 cycles, respectively, which are 60%, 77%, and 111% higher than their counterparts. This work offers a new route to improve the electrochemical performance of high sulfur loading electrodes and contribute to the future commercialization and practical application of Li-S batteries.

Experimental Section ((delete section if not applicable))

Detailed information is in the Supporting Experimental Section of the Supporting Information.

Supporting Information ((delete if not applicable))
Supporting Information is available from the Wiley Online Library or from the author.

Acknowledgements

This research was supported by the Natural Science and Engineering Research Council of Canada (NSERC), the Canada Research Chair Program (CRC), the Canada Foundation for Innovation (CFI), and the University of Western Ontario (UWO), National Natural Science Foundation of China (No. 51403209, 51677176, 51673199, 21406221, 51177156/E0712), Youth Innovation Promotion Association (2015148), Natural Sciences Foundation of Liaoning Province of China (2013020126), Youth Innovation Foundation of Dalian Institute of Chemical Physics (201307), Xiaofei Yang, Xuejie Gao, Jianneng Liang and Xiaoting Lin are supported by the Chinese Scholarship Council.

Statement of Contributions
X. Y. and X. G. contributed equally to this work. X. Y. and X. G. conceived and designed the experimental work and prepared the manuscript; Y. Y., X. L. and J. L. helped with TEM, SEM and XRD characterization; Dr. Y. Z. helped with ALD coating, S. P. J., L. K., J. R., P. K. helped with DFT calculation; X. L., M. N. B., Y. H. and T. -K. S. performed the XANES characterization and analyzed the XANES data; K. A., X. L. and R. L. participated in the discussion of the data; H. Z., H. Z. and X. S. supervised the overall project. All authors have given approval to the final version of the manuscript.

Received: ((will be filled in by the editorial staff))
Revised: ((will be filled in by the editorial staff))
Published online: ((will be filled in by the editorial staff))

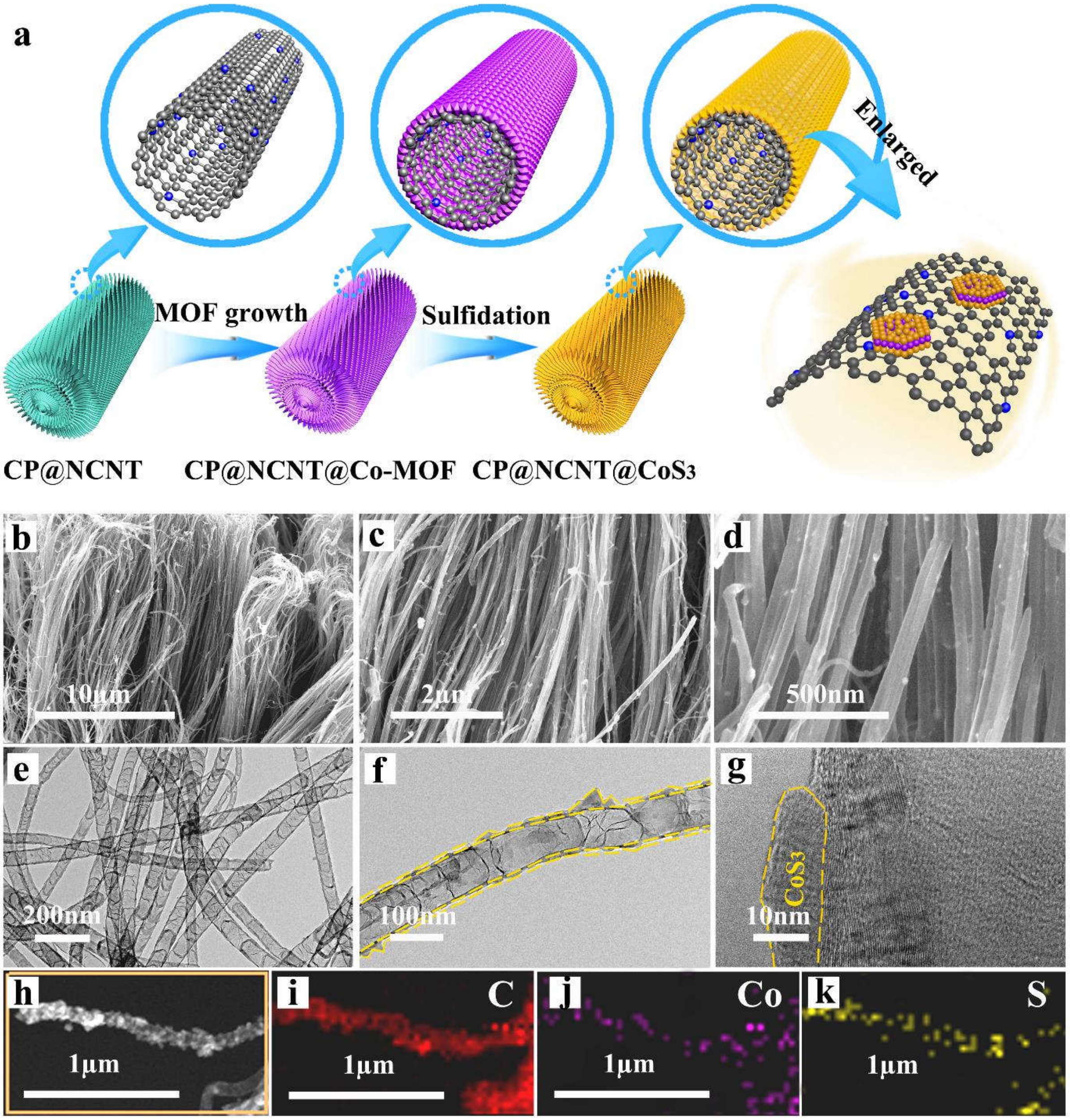

Figure 1. (a) Schematic illustration of CP@NCNT@CoS_3 preparation, (b-d) SEM images and (e-g) TEM images of CP@NCNT@CoS_3 at different magnifications, and (h-k) STEM image of CP@NCNT@CoS_3 and corresponding elemental mappings of C, Co and S.

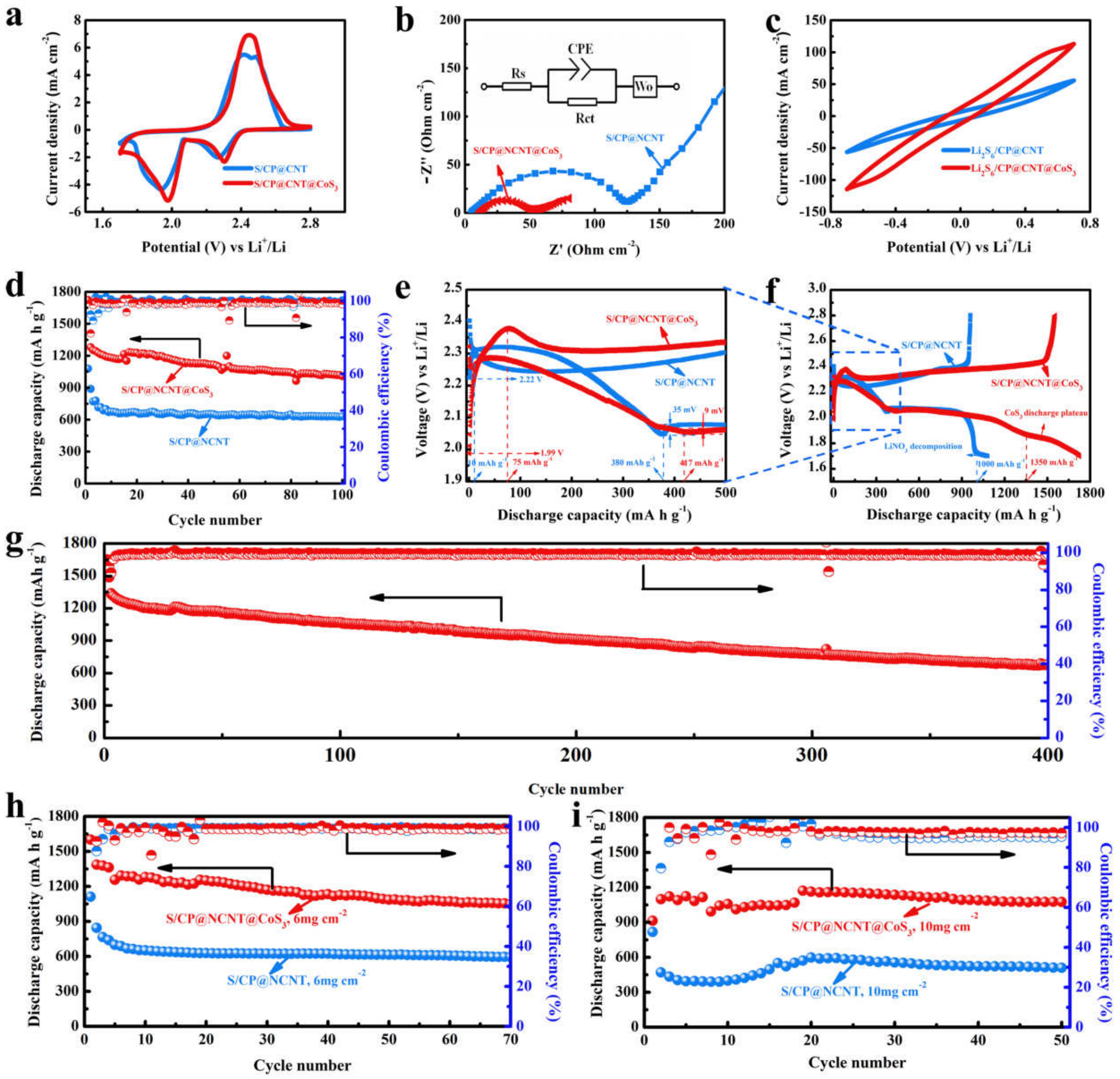

Figure 2. (**a**) CV curves, (**b**) EIS plots and (**c**) symmetrical Li_2S_6–Li_2S_6 cells of S/CP@NCNT@CoS_3 and S/CP@NCNT electrodes. (**d**) Cycling performance and (**e-f**) Charge/discharge curves of 3 mg cm^{-2} sulfur loaded S/CP@NCNT@CoS_3 and S/CP@NCNT electrodes at 1.3 mA cm^{-2}. (**g**) Cycling stability of 3 mg cm^{-2} sulfur loaded S/CP@NCNT@CoS_3 at 4 mA cm^{-2}. The cycling performance of (**h**) 6 mg cm^{-2} and (**i**) 10 mg cm^{-2} sulfur loaded S/CP@NCNT@CoS_3 electrodes at 1.3 mA cm^{-2}.

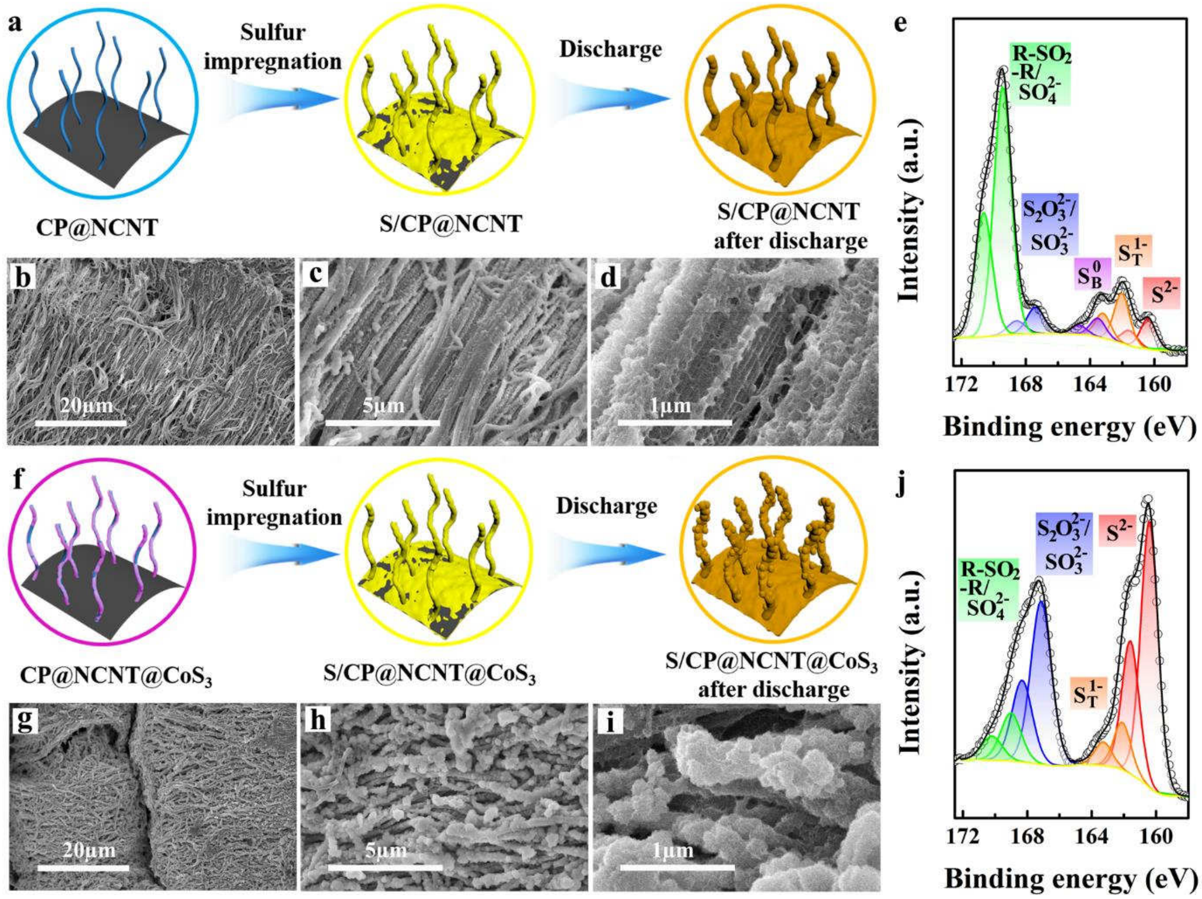

Figure 3. Schematic illustration of (**a**) S/CP@NCNT and (**f**) S/CP@NCNT@CoS$_3$ electrodes during discharge. SEM images of (**b-d**) S/CP@NCNT and (**g-i**) S/CP@NCNT@CoS$_3$ electrodes after first discharge at different magnifications. XPS analysis of the discharge products on (**e**) S/CP@NCNT and (**j**)S/CP@NCNT@CoS$_3$.

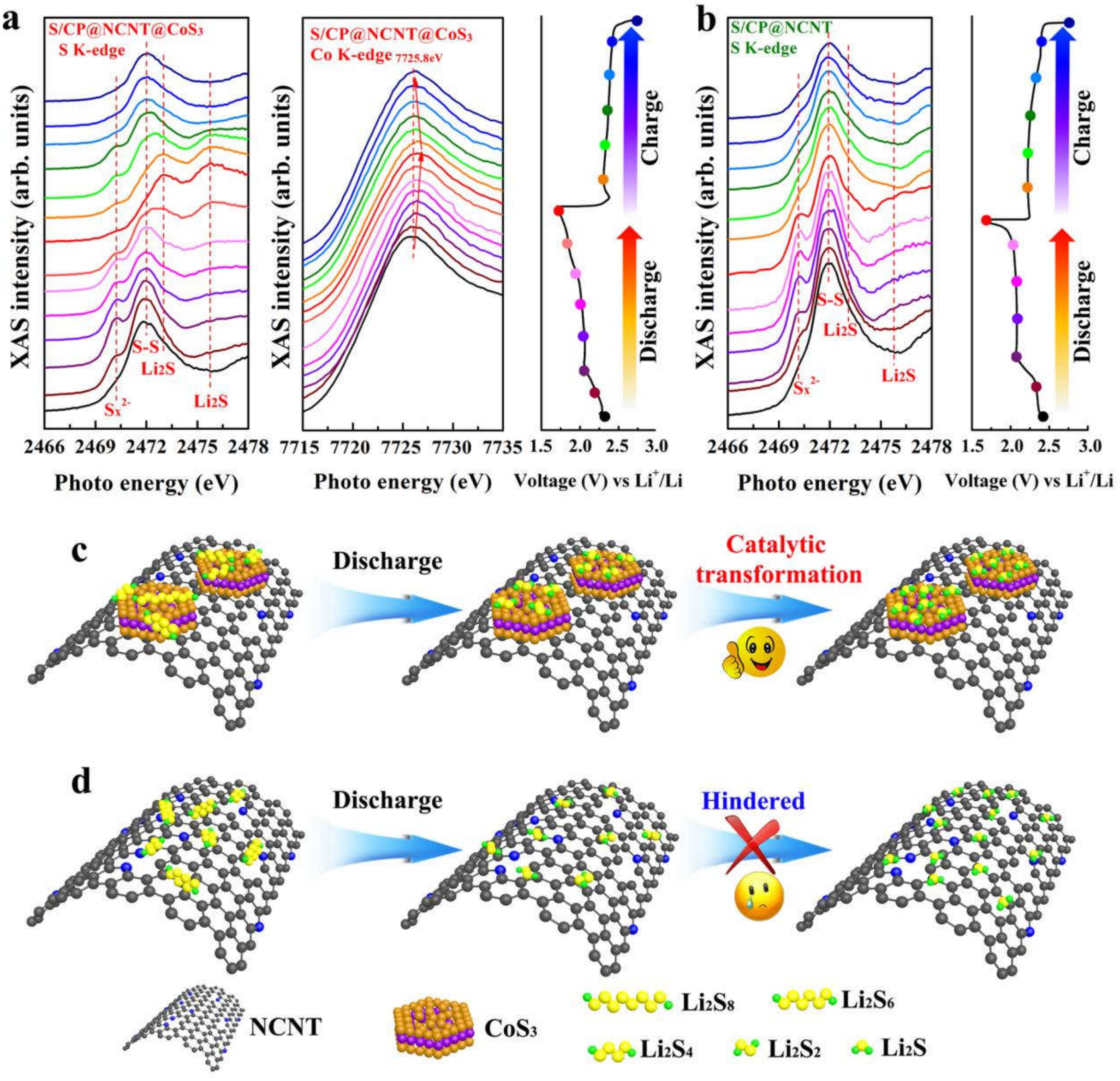

Figure 4. (**a**) Sulfur K-edge and cobalt K-edge XANES of S/CP@NCNT@CoS$_3$ electrode at different depth of discharge/charge. (**b**) Sulfur K-edge of S/CP@NCNT electrode at different depth of discharge/charge. Schematic illustration of sulfur species transformation on (**c**) CP@NCNT@CoS$_3$ and (**d**) CP@NCNT.

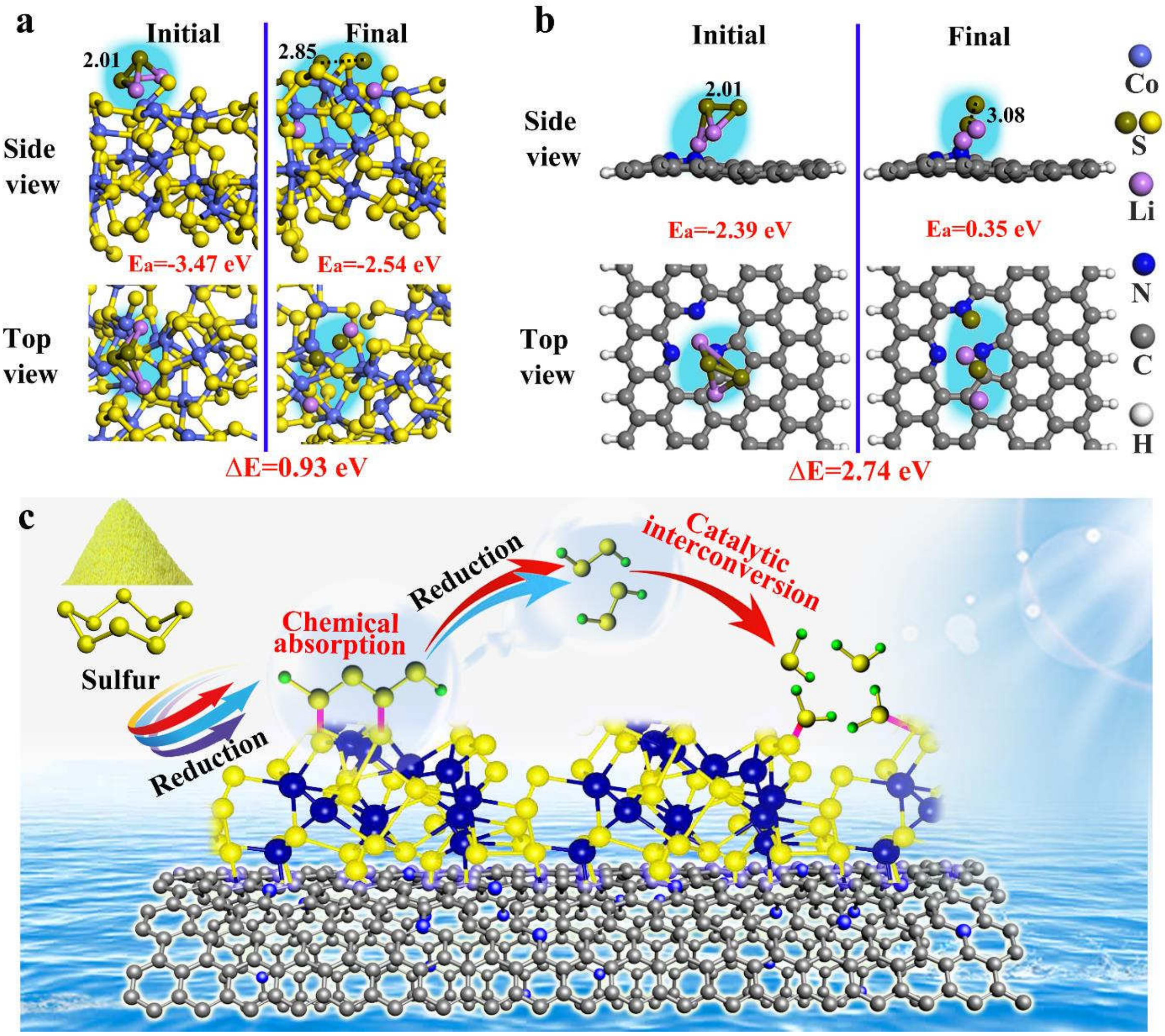

Figure 5. The absorption energy (Ea) and dissociation energy (ΔE) of Li_2S_2 on the surface of (**a**) CoS_3 and (**b**) NCNT. (**c**) Schematic illustration of the reaction process of sulfur on the CoS_3 catalyst.

Amorphous CoS$_3$ were developed to promote the the solid-solid conversion from solid-state intermediate product Li$_2$S$_2$ to the final discharge product Li$_2$S, which significantly increased the sulfur utilizations for over 20% for high loading electrodes.

Keywords

Amorphous cobalt sulfide; High loading; Catalytic effect; High utilization; Lithium-sulfur batteries;

Xiaofei Yang+, Xuejie Gao+, Qian Sun, Sara Panahian Jand, Ying Yu, Yang Zhao, Xia Li, Keegan Adair, Liang-Yin Kuo, Jochen Rohrer, Jianneng Liang, Xiaoting Lin, Mohammad Norouzi Banis, Yongfeng Hu, Hongzhang Zhang, Xianfeng Li, Ruying Li, Huamin Zhang*, Payam Kaghazchi, Tsun-Kong Sham, Xueliang Sun**

Promoting the Transformation of Li$_2$S$_2$ to Li$_2$S: Significantly Increasing Utilization of Active Materials for High Sulfur Loading Li-S Batteries

TOC figure

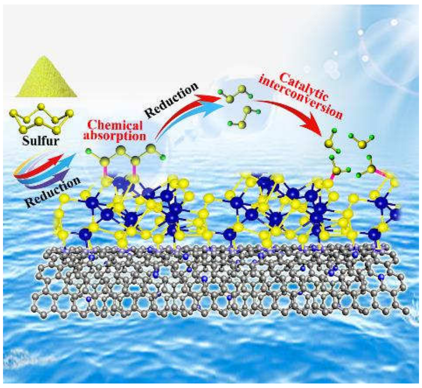

[1] a) A. Manthiram, Y. Fu, S. H. Chung, C. Zu, Y. S. Su, *Chemical Rev.* 2014, **114**, 11751; b) Z. W. Seh, Y. Sun, Q. Zhang, Y. Cui, *Chem. Soc. Rev.* 2016, **45**, 5605.
[2] X. Yang, X. Li, K. Adair, H. Zhang, X. Sun, *Electrochem. Energy Rev.* 2018, **1**, 239.
[3] S. Gu, C. Sun, D. Xu, Y. Lu, J. Jin, Z. Wen, *Electrochem. Energy Rev.* 2018, **1**, 599.
[4] a) X. Yang, H. Zhang, Y. Chen, Y. Yu, X. Li, H. Zhang, *Nano Energy* 2017, **39**, 418; b) Y. Qiu, W. Li, W. Zhao, G. Li, Y. Hou, M. Liu, L. Zhou, F. Ye, H. Li, Z. Wei, S. Yang, W. Duan, Y. Ye, J. Guo, Y. Zhang, *Nano Lett.* 2014, **14**, 4821; c) X. Yang, N. Yan, W. Zhou, H. Zhang, X. Li, H. Zhang, *J. Mater. Chem. A* 2015, **3**, 15314. d) S. Feng, J. Song, S. Fu, C. Zhu, Q. Shi, M.-K. Song, D. Du, Y. Lin, J. *Mater. Chem. A* 2017, **5**, 23737.
[5] a) S. Lu, Y. Cheng, X. Wu, J. Liu, *Nano Lett.* 2013, **13**, 2485; b) X. Yang, B. Dong, H. Zhang, R. Ge, Y. Gao, H. Zhang, *RSC Adv.* 2015, **5**, 86137.
[6] T. Tang, Y. Hou, *Electrochem. Energy Rev.* 2018, **1**, 403.
[7] X. Ji, L. F. Nazar, *J. Mater. Chem.* 2010, **20**, 9821.
[8] a) C. Barchasz, F. Molton, C. Duboc, J. C. Lepretre, S. Patoux, F. Alloin, Anal. Chem. 2012, 84, 3973; b) K. Sun, H. Liu, H. Gan, *J. Electrochem. En. Conv. Stor.* 2016, **13**, 021002.
[9] X. Yang, Y. Chen, M. Wang, H. Zhang, X. Li, H. Zhang, *Adv. Funct. Mater.* 2016, **26**, 8427.
[10] a) Y. Yu, H. Zhang, X. Yang, Y. Chen, Z. Jia, J. Yan, H. Zhang, X. Li, *J. Mater. Chem. A* 2018, **6**, 24066; b) Y. Yu, H. Zhang, X. Yang, J. Gou, X. Tong, X. Li, H. Zhang, *Energy Storage Mater.* 2018, https://doi.org/10.1016/j.ensm.2018.07.015; c) S. Feng, J. Song, C. Zhu, Q. Shi, D. Liu, J. Li, D. Du, Q. Zhang, Y. Lin, *ACS Appl. Mater. Interfaces* 2019, **11**, 5911.
[11] X. Zhao, J. Jiang, Z. Xue, C. Yan, T. Mu, *Chem. Commun.* 2017, **53**, 9418.
[12] a) A. Sakuda, K. Ohara, K. Fukuda, K. Nakanishi, T. Kawaguchi, H. Arai, Y. Uchimoto, T. Ohta, E. Matsubara, Z. Ogumi, T. Okumura, H. Kobayashi, H. Kageyama, M. Shikano, H. Sakaebe, T. Takeuchi, *J. Am. Chem. Soc.* 2017, **139**, 8796; b) H. Ye, L. Ma, Y. Zhou, L. Wang, N. Han, F. Zhao, J. Deng, T. Wu, Y. Li, J. Lu, *Proc. Natl. Acad. Sci. U.S.A.* 2017, **114**, 13091.
[13] a) Q. Guo, Y. Ma, T. Chen, Q. Xia, M. Yang, H. Xia, Y. Yu, *ACS Nano* 2017, **11**, 12658; b) J. D. Benck, Z. Chen, L. Y. Kuritzky, A. J. Forman, T. F. Jaramillo, *ACS Catal.* 2012, **2**, 1916; c) L. R. L. Ting, Y. Deng, L. Ma, Y.-J. Zhang, A. A. Peterson, B. S. Yeo, *ACS Catal.* 2016, **6**, 861; d) N. Kornienko, J. Resasco, N. Becknell, C. M. Jiang, Y. S. Liu, K. Nie, X. Sun, J. Guo, S. R. Leone, P. Yang, *J. Am. Chem. Soc.* 2015, **137**, 7448.
[14] H.-J. Peng, W.-T. Xu, L. Zhu, D.-W. Wang, J.-Q. Huang, X.-B. Cheng, Z. Yuan, F. Wei, Q. Zhang, *Adv. Funct. Mater.* 2016, **26**, 6351.
[15] X. Yang, Y. Yu, N. Yan, H. Zhang, X. Li, H. Zhang, *J. Mater. Chem. A* 2016, **4**, 5965.
[16] Y. Li, K. K. Fu, C. Chen, W. Luo, T. Gao, S. Xu, J. Dai, G. Pastel, Y. Wang, B. Liu, J. Song, Y. Chen, C. Yang, L. Hu, *ACS Nano* 2017, **11**, 4801.
[17] Z. Yuan, H. J. Peng, T. Z. Hou, J. Q. Huang, C. M. Chen, D. W. Wang, X. B. Cheng, F. Wei, Q. Zhang, *Nano Lett.* 2016, **16**, 519.
[18] a) X. Gao, X. Yang, M. Li, Q. Sun, J. Liang, J. Luo, J. Wang, W. Li, J. Liang, Y. Liu, S. Wang, Y. Hu, Q. Xiao, R. Li, T.-K. Sham, X. Sun, *Adv. Funct. Mater.* 2019, **29**,1806724; b) S. Feng, H. Zhong, J. Song, C. Zhu, P. Dong, Q. Shi, D. Liu, J. Li, Y.-C. Chang, S. P. Beckman, M.-k. Song, D. Du, Y. Lin, *ACS Appl. Energy Mater.* 2018, **1**, 7014.
[19] X. Yang, Y. Yu, X. Lin, J. Liang, K. Adair, Y. Zhao, C. Wang, X. Li, Q. Sun, h. zhang, X. Li, R. Li, H. Zhang, X. Sun, *J. Mater. Chem. A* 2018, **6**, 22958.
[20] J. Park, E. T. Kim, C. Kim, J. Pyun, H.-S. Jang, J. Shin, J. W. Choi, K. Char, Y.-E. Sung, *Adv. Energy Mater.* 2017, **7**, 1700074.
[21] a) J. Liu, Z. Bao, Y. Cui, E. J. Dufek, J. B. Goodenough, P. Khalifah, Q. Li, B. Y. Liaw, P. Liu, A. Manthiram, Y. S. Meng, V. R. Subramanian, M. F. Toney, V. V. Viswanathan, M. S. Whittingham, J. Xiao, W. Xu, J. Yang, X.-Q. Yang, J.-G. Zhang, *Nat. Energy* 2019, **4**, 180;

D. Lu, Q. Li, J. Liu, J. Zheng, Y. Wang, S. Ferrara, J. Xiao, J. G. Zhang, J. Liu, *ACS Appl. Mater. Interfaces* 2018, **10**, 23094.
[22] a) R. Elazari, G. Salitra, A. Garsuch, A. Panchenko, D. Aurbach, *Adv. Mater.* 2011, 23, 5641; b) M. Wang, W. Wang, A. Wang, K. Yuan, L. Miao, X. Zhang, Y. Huang, Z. Yu, J. Qiu, *Chem. Commun.* 2013, **49**, 10263; c) W. Zhou, H. Chen, Y. Yu, D. Wang, Z. Cui, F. J. DiSalvo, H. D. Abru~na, *ACS Nano* 2013, **7**, 8801; d) C. Zu, A. Manthiram, *Adv. Energy Mater.* 2014, **4**, 1400897; e) Z. Li, J. T. Zhang, Y. M. Chen, J. Li, X. W. Lou, *Nat. Commun.* 2015, **6**, 8850; f) A. Schneider, C. Suchomski, H. Sommer, J. Janek, T. Brezesinski, *J. Mater. Chem. A* 2015, **3**, 20482; g) Q. Sun, X. Fang, W. Weng, J. Deng, P. Chen, J. Ren, G. Guan, M. Wang, H. Peng, *Angew. Chem. Int. Ed.* 2015, **54**, 10539; h) C. H. Chang, S. H. Chung, A. Manthiram, *Small* 2016, **12**, 174; i) N. He, L. Zhong, M. Xiao, S. Wang, D. Han, Y. Meng, *Sci. Rep.* 2016, **6**, 33871; j) X. Li, X. Pu, S. Han, M. Liu, C. Du, C. Jiang, X. Huang, T. Liu, W. Hu, *Nano Energy* 2016, **30**, 193; k) F. Nitze, M. Agostini, F. Lundin, A. E. Palmqvist, A. Matic, *Sci. Rep.* 2016, **6**, 39615; l) J. Wang, S. Cheng, W. Li, S. Zhang, H. Li, Z. Zheng, F. Li, L. Shi, H. Lin, Y. Zhang, *J. Power Sources* 2016, **321**, 193; m) H. Xu, L. Qie, A. Manthiram, *Nano Energy* 2016, **26**, 224; n) C.-H. Chang, S.-H. Chung, A. Manthiram, *Mater. Horiz.* 2017, **4**, 249; o) S. Li, T. Mou, G. Ren, J. Warzywoda, Z. Wei, B. Wang, Z. Fan, *J. Mater. Chem. A* 2017, **5**, 1650; p) J. Liu, D. G. D. Galpaya, L. Yan, M. Sun, Z. Lin, C. Yan, C. Liang, S. Zhang, *Energy Environ. Sci.* 2017, **10**, 750; q) Y. Mao, G. Li, Y. Guo, Z. Li, C. Liang, X. Peng, Z. Lin, *Nat. Commun.* 2017, **8**, 14628; r) H. Xu, A. Manthiram, *Nano Energy* 2017, **33**, 124; s) K. Zhang, K. Xie, K. Yuan, W. Lu, S. Hu, W. Wei, M. Bai, C. Shen, *J. Mater. Chem. A* 2017, **5**, 7309; t) X. Hong, J. Jin, T. Wu, Y. Lu, S. Zhang, C. Chen, Z. Wen, *J. Mater. Chem. A* 2017, **5**, 14775; u) F. Qin, X. Wang, K. Zhang, J. Fang, J. Li, Y. Lai, *Nano Energy* 2017, **38**, 137; v) F. Zeng, A. Wang, W. Wang, Z. Jin, Y.-S. Yang, *J. Mater. Chem. A* 2017, **5**, 12879.
[23] a) A. Eftekhari, *Sustainable Energy Fuels* 2017, **1**, 2053; b) A. Eftekhari, *Adv. Energy Mater.* 2018, **8**, 1801156.
[24] a) M. I. Nandasiri, L. E. Camacho-Forero, A. M. Schwarz, V. Shutthanandan, S. Thevuthasan, P. B. Balbuena, K. T. Mueller, V. Murugesan, *Chem. Mater.* 2017, **29**, 4728; b) X. Liang, C. Hart, Q. Pang, A. Garsuch, T. Weiss, L. F. Nazar, *Nat. Commun.* 2015, **6**, 5682.
[25] Z. Lin, C. Nan, Y. Ye, J. Guo, J. Zhu, E. J. Cairns, *Nano Energy* 2014, **9**, 408.
[26] X. Feng, M. K. Song, W. C. Stolte, D. Gardenghi, D. Zhang, X. Sun, J. Zhu, E. J. Cairns, J. Guo, *Phys. Chem. Chem. Phys.* 2014, **16**, 16931.
[27] M. Cuisinier, P.-E. Cabelguen, S. Evers, G. He, M. Kolbeck, A. Garsuch, T. Bolin, M. Balasubramanian, L. F. Nazar, *J. Phys. Chem. Lett.* 2013, **4**, 3227.
[28] M. U. Patel, I. Arcon, G. Aquilanti, L. Stievano, G. Mali, R. Dominko, *ChemPhysChem* 2014, **15**, 894.
[29] M. Vijayakumar, N. Govind, E. Walter, S. D. Burton, A. Shukla, A. Devaraj, J. Xiao, J. Liu, C. Wang, A. Karim, S. Thevuthasan, *Phys. Chem. Chem. Phys.* 2014, **16**, 10923.